

TEXTURE AND MICROSTRUCTURE ANALYSIS WITH HIGH-ENERGY SYNCHROTRON RADIATION

Hans J. Bunge

Department of Physics and Physical Technologies, TU Clausthal, Leibniz str. 4, D-38678 Clausthal-Zellerfeld, Germany

ABSTRACT

Diffraction of high-energy synchrotron radiation with wavelengths in the range of 0.1Å, provided by the beamline BW5 at HASYLAB in Hamburg, was used to measure textures (orientation distribution) and microstructures (spatial distribution) of the crystallites in various polycrystalline materials. In order to achieve extremely high angular- combined with very high lateral resolution a continuous sweeping technique with an area detector was employed. This technique "images" three different types of two-dimensional sections and projections of the six-dimensional orientation-location space onto the area detector. In many cases the orientations and locations of all individual grains of the sample can thus be seen simultaneously. The high penetration depth of this radiation in the range of several centimeters (comparable with that of neutrons) allows investigating big or capsulated samples. Examples are given of grain-resolved recrystallization textures, a soldering seam, a filled beverage can, and the orientation distribution of kamacite lamellae in an iron meteorite, elucidating the orientation relationship of the γ→α transformation in iron.

INTRODUCTION

The *texture* of a polycrystalline material is defined by the orientation distribution function f(g) of the crystallites, where g is crystal orientation, e.g. expressed in terms of the Euler angles $g = \{\varphi_1 \Phi \varphi_2\}$ [1]. The *microstructure* specifies crystal orientation g(x) at any point $x = \{x_1 x_2 x_3\}$ in the material [2]. In between these two definitions we may consider the *local texture* f(g,X) in a volume element bigger than grain size at the position $X = \{X_1 X_2 X_3\}$ [3]. These three quantities are illustrated in Figure 1.

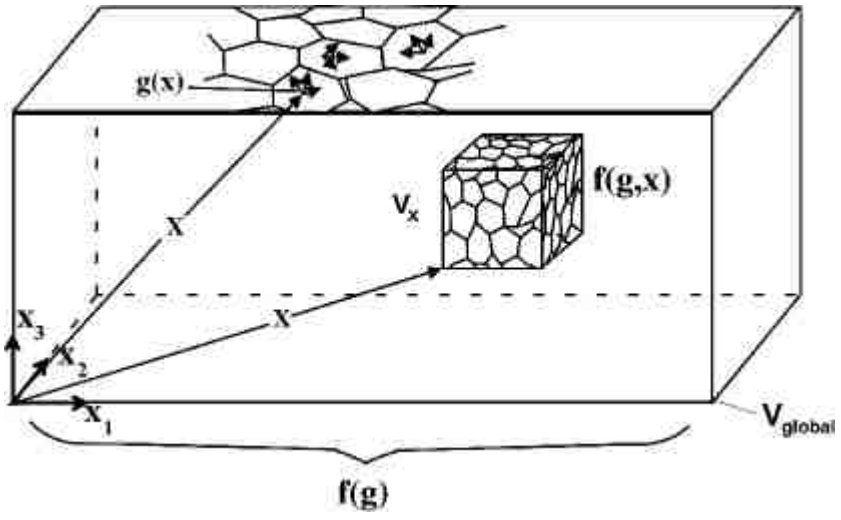

Figure 1.
Illustration of texural and microstructural quantities
a) the global texture f(g)
b) the local texture f(g,X)
c) the local orientation g(x)

This document was presented at the Denver X-ray Conference (DXC) on Applications of X-ray Analysis.

Sponsored by the International Centre for Diffraction Data (ICDD).

This document is provided by ICDD in cooperation with the authors and presenters of the DXC for the express purpose of educating the scientific community.

Usage is restricted for the purposes of education and scientific research.

DXC Website
– www.dxcicdd.com

ICDD Website
- www.icdd.com

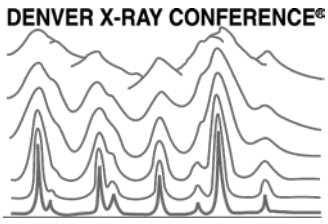

In all three quantities the resolving power in the orientation space respectively location space is important. It depends strongly on the experimental technique by which the quantities are being measured. These are particularly X-ray-, neutron-, or electron diffraction which has very different values of the two resolving powers. Further, X-rays may be generated by conventional X-ray tubes or by synchrotron sources with extremely different orientation as well as location resolving powers.

A third important property of the radiations is their penetration depth in matter. This is lowest for electrons, medium for "conventional" X-rays with wavelengths in the order of 1Å, and highest for neutrons and high-energy synchrotron radiation with wavelengths in the order of 0.1 Å. With respect to these three characteristic features HE-synchrotron radiation is outstanding in as far as it allows extremely high orientation resolution (e.g. 0.01° or even better) [4], very high lateral resolution (e.g. 10 μm or better) [5], and very high penetration depth (e.g. 1–10 cm).

In order to actually reach highest orientation- as well location resolution the conventional step scanning techniques had to be replaced by continuous "sweeping" techniques using a continuously moving area detector. This technique was introduced long time ago with photographic film as the only available area detector at that time, as was reviewed by Wassermann and Grewen [6]. It became, however, really practicable only with an electronically readable area detector.

In order to obtain all three orientation parameters the "projection" problem in the orientation space, resulting from the indistinguishable rotation about the diffraction vector, must be solved by combining several diffraction vectors.

In order to obtain all three spatial parameters the projection problem in the direct space, resulting from projection along the incident beam, must be solved by using incident beams in different sample directions.

THE INSTRUMENT

We used particularly the diffraction installation at the beamline BW5 at the storage ring DORIS at HASYLAB/DESY in Hamburg described by Bouchard et al. [7]. The original white spectrum of the synchrotron beam is monochromatized by an absorber which eliminates the long-wave part, followed by a crystal monochromator which selects a wavelengths in the order of 0.1 Å. The long distance between source and sample (~ 40 m) leads to the extreme parallelism of the beam and hence to the extreme orientation resolution. The extremely high intensity allows to use very narrow entrance slits and hence to reach very high lateral resolution [8].

The instrument is equipped with an area detector (presently an image plate detector) which can be continuously shifted *during exposure*. In between sample and detector two different slit systems can be used alternatively:

The *diffraction angle slit system,* shown schematically in Figure 2, allows only an arc (<180°) of one selected Debye-Scherrer cone to reach the detector. When the detector is shifted continuously during exposure the intensity of the diffraction ring is spread out over a two-dimensional area of the detector, which is then being read out after exposure is finished. Simultaneously the sample can be rotated or translated which may change the intensity distribution along the angle γ of the Debye-Scherrer ring.

The *diffraction plane slit system* is shown in Figure 3a. It fixes the diffraction plane but it allows all reflection angles to pass through. For this purpose the incident beam must be narrow in the direction y but it can be as high as possible in the direction z, if only the distance to the detector is long enough to avoid overlapping of different (hkl). Figure 3b shows diffraction in this plane at those grains in the sample which are in reflection orientation for the diffraction vector S with the sample in the orientation ω. When detector and sample are being continuously shifted in the direction y during exposure then this technique images the y-z coordinates of all these grains (positions and shapes). It does not see, however, the x-coordinates, i.e. the image is a projection in this direction.

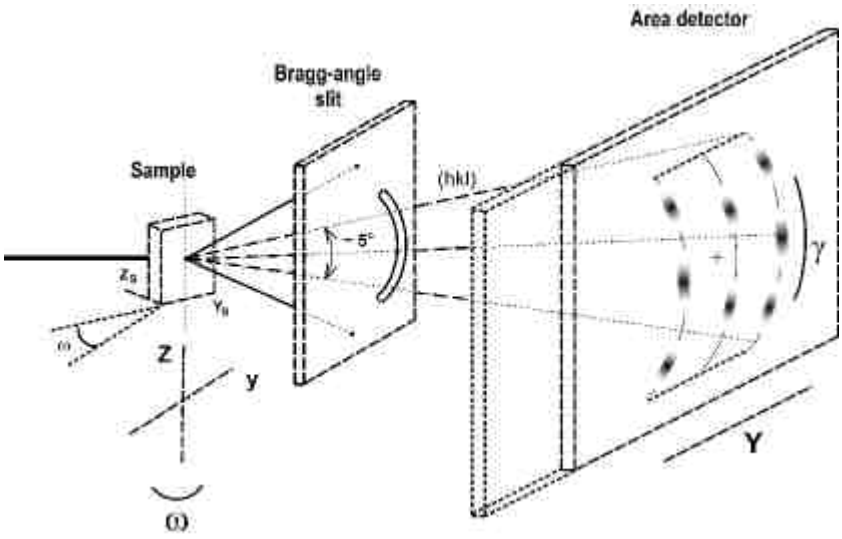

Figure 2. Texture diffractometer with the diffraction angle slit system and "moving" detector

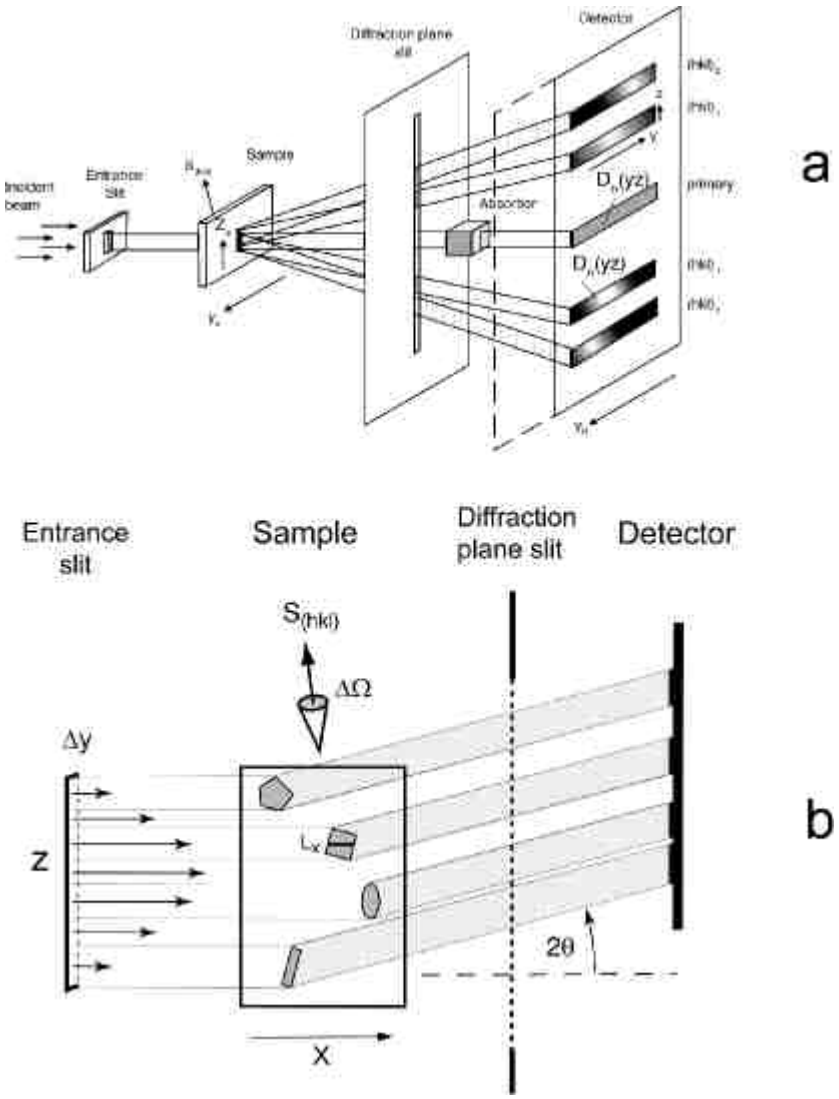

Figure 3. Texture diffractometer with the diffraction plane slit system and "moving" detector (schematic).
a) The entrance slit selects a thin, band-like primary beam. The diffraction plane slit selects several thin, band-like reflected beams which are imaged in the detector as a function of the position y in the sample.
b) Grains which are in reflection orientation with the diffraction vector $S_{(hkl)}$ give rise to reflected bands according to their diameters in z-direction.

RESULTS

Rotation of the sample through the angle ω in Figure 2 is thus "imaged" along the coordinate y of the detector. The coordinates {ωγ} in the image specify the position of the diffraction vector in the sample. Hence, the {ωγ}-distribution of the intensity in Figure 4 corresponds to a *pole figure* expressed in terms of these two angular coordinates. Figure 4a and b show two examples of that, i.e. the (111)-pole figures of a cold rolled and a recrystallized nickel sheet, respectively. In Figure 4b the orientations of individual grains are resolved which is shown in higher magnification in Figure 4c.

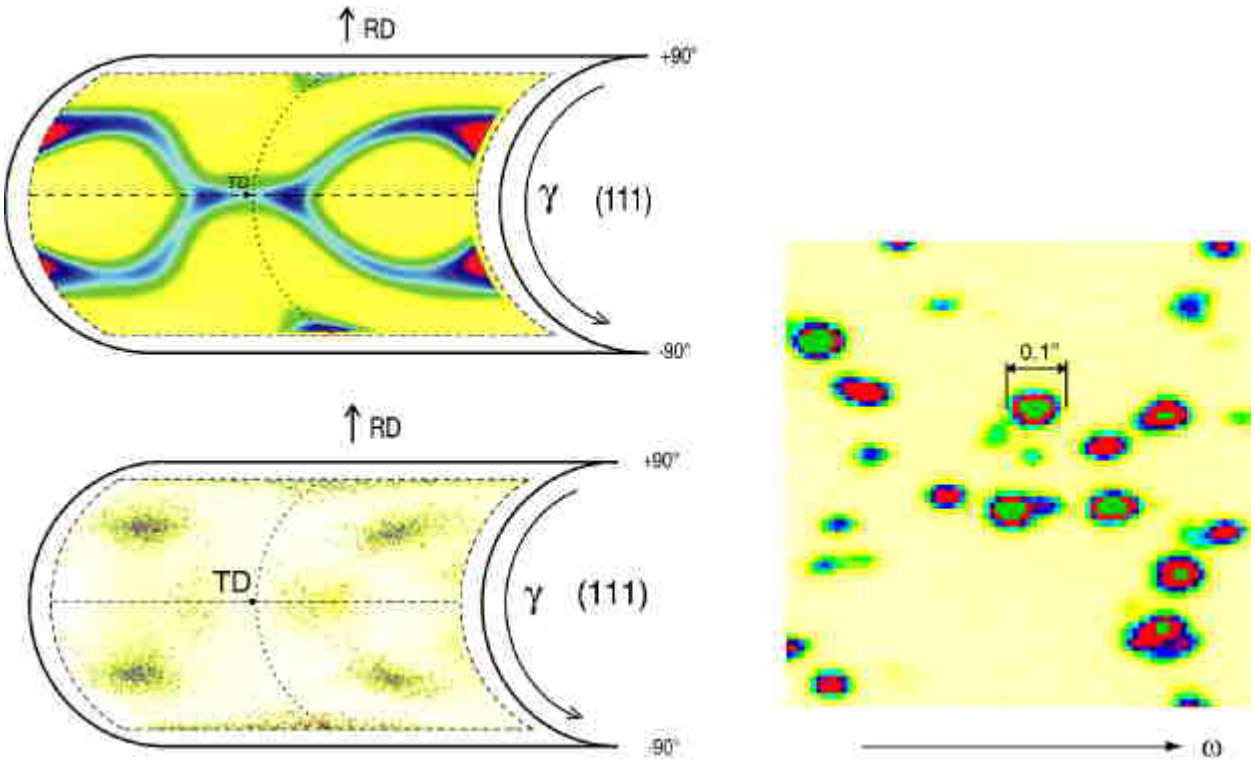

Figure 4. Pole density distribution diagrams (pole figures) of the <111> directions of nickel.
a) cold rolled; b) recrystallized; c) a magnification of a local area of Figure 4b.

Translation of the sample in the direction y "images" the local variation of the texture in the sample in this direction. Figure 5b shows the local variation of intensity (as a function of the angle γ) in the direction y of the sample shown in Figure 5a. This is a "lamellar" copper tube (used as a heat exchanger) which has very different texture in the body of the tube and in the lamellae. Figure 6 shows the analogous image (i.e. a location scan in y-direction) of a recrystallized nickel sheet. In this case individual grains are resolved. A grain reflects X-rays as long as it passes through the primary beam. Hence, Figure 6 reveals the positions as well as the diameters (in y-direction) of grains which are in reflection orientation with the diffraction vector S in the sample direction specified by {ωγ}

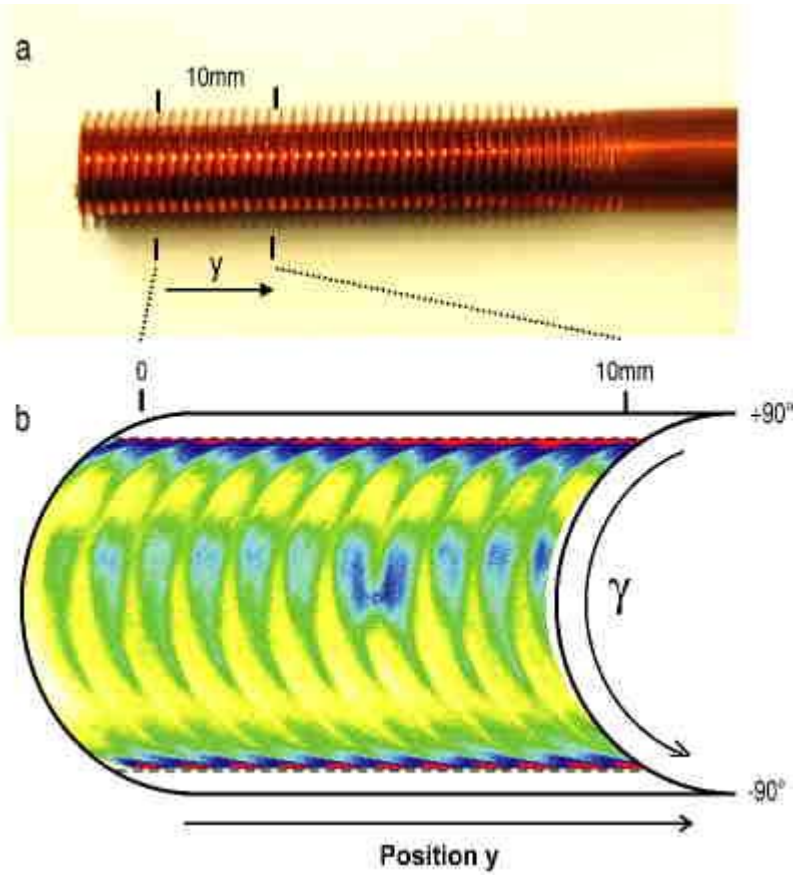

Figure 5.
Location image of an inhomogeneous texture.
a) A lamellar copper tube (heat exchanger tube).
b) Diffracted intensity at the angle γ imaged along the axis direction y of the tube.

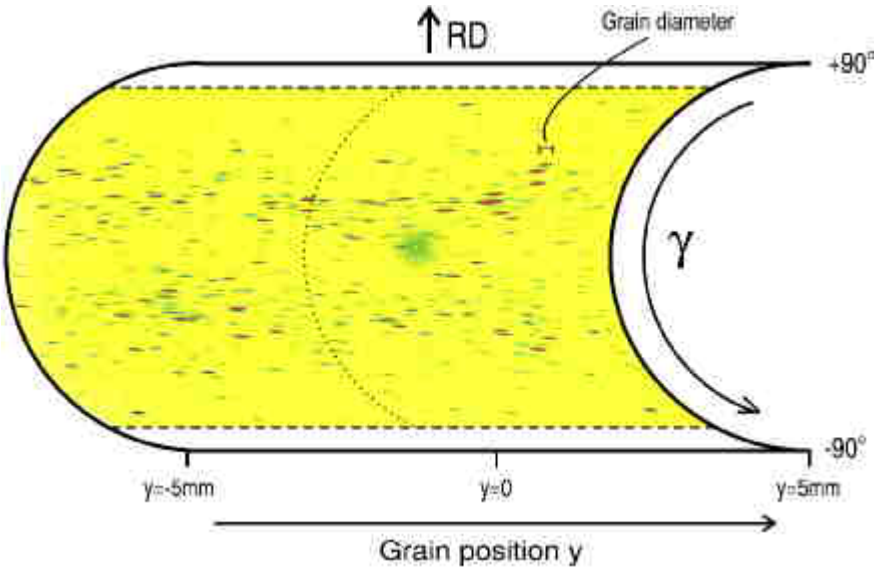

Figure 6.
Location image of individual grains of a recrystallized nickel sheet showing grains which are in reflection orientation under the angle γ at the position y in the sample.

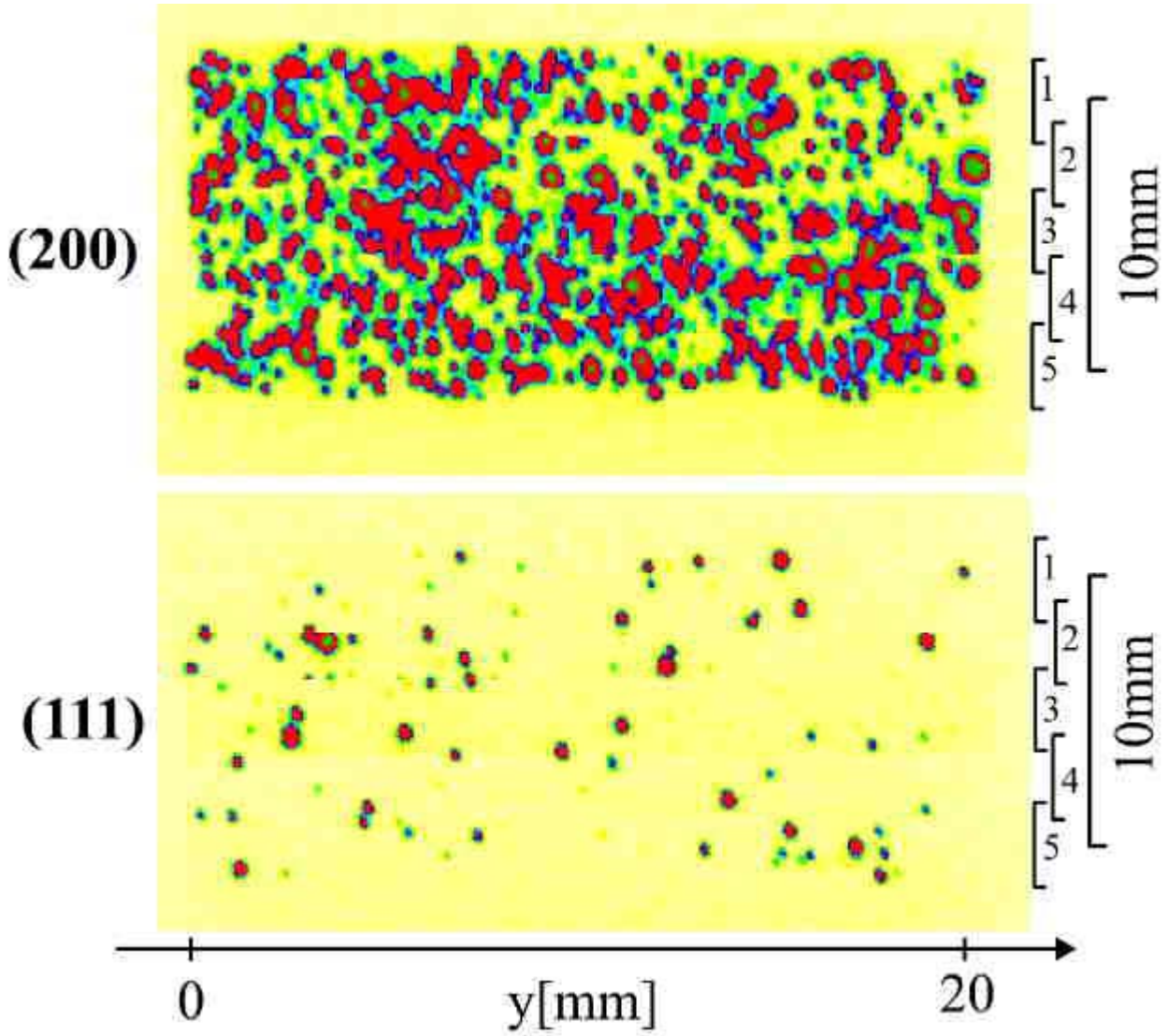

Figure 7. Projected cross-sections of grains of a recrystallized nickel sheet imaged with the method of Figure 3. The images are fit together of fife (narrower) partial images. (This was necessary because of the limited height of the beam in z-direction).

Figure 7 shows the (projected) cross-sections of the grains of a recrystallized nickel sheet measured with fixed diffraction vectors for (111) and (200) respectively, using this time, the *diffraction plane slit system* shown in Figure 3. Grains with other orientations are invisible (translucent) in this technique. (The two images in Figure 7 are composed of fife individual strips of 3 mm height fit together in order to cover a total area of 12 × 20 mm).

The same technique can also be used in *multi-phase materials*. As an example Figure 8 shows a scan over a soldering seam consisting of an fcc-alloy, connecting two halves of iron sheet with bcc-structure. One sees the different grain structure in the seam, the heat-influenced zone and the non-influenced iron sheets.

A *special method* of texture imaging is shown in Figure 9. The sample is a beverage can [9]. The diffraction-angle slit was wide enough to allow diffracted beams (of the same lattice planes (hkl)) from the front and rear wall to reach the detector. (However, also separation of both is possible).

The sample was rotated around its axis which corresponds to a *location image along the circumference* of the can. The penetration depth of the short-wave X-ray beam is high enough to penetrate the liquid content of the can, as well. (The liquid is mainly water. Hence, having the high incoherent scattering of neutrons in water in mind, the analogous technique cannot be used with neutrons). This last example was chosen here in order to demonstrate the advantages of high-energy synchrotron radiation for texture and microstructure analysis as well as for *fast inspection* of big, multicomponent samples or even *complex technological structural units.*

A further example of a pole figure measured with the technique of Figure 2 with high angular resolution is shown in Figure 10a. The sample was an iro-nickel meteorite of the Gibeon fall (octahedrite). It consists mainly of α-FeNi (Kamacite) which was formed by (diffusive) phase transformation from γ-FeNi (Taenite) during very slow cooling in the range from ~800°C to 400°C with a cooling rate of ~1K/10^6 years. The original Taenite was (presumably) a big

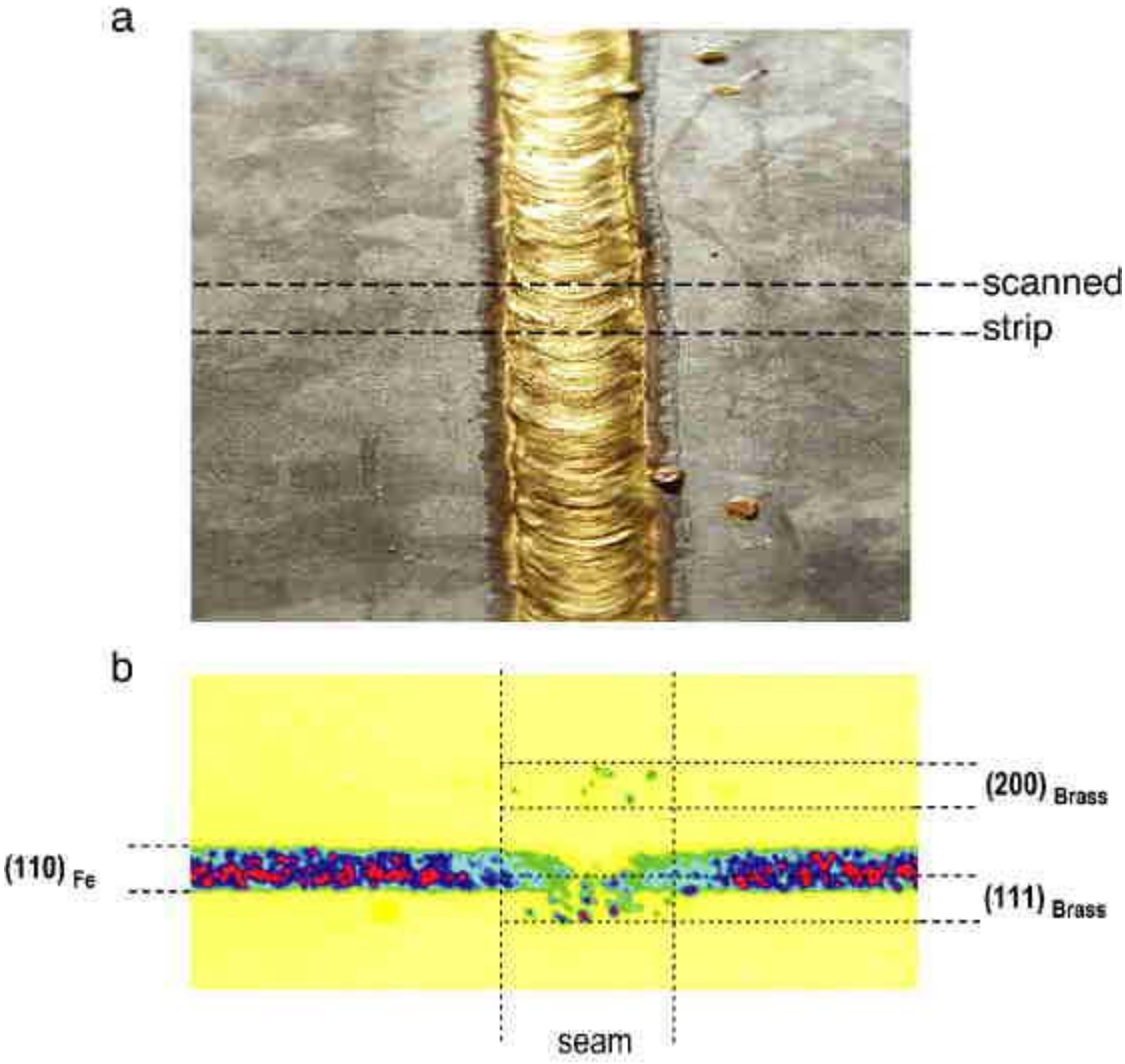

Figure 8. Projected cross-sections of grains of an iron sheet with a soldering seam consisting of a brass-type soldering alloy. The image shows grains of this material in (111) and (200) reflection orientation as well as Fe-grains in (110)-reflection orientation. This image reveals clearly the heat-influenced zone of the iron sheet.

monocrystal which transformed into Kamacite in the form of Widmannstätten plates with definite orientation relationship with respect to the orientation of the Taenite crystal [10]. For this orientation relationship two different models were discussed in the literature, i.e. the Kurdjumov-Sachs and the Nishiyama-Wassermann model, respectively. Figure 10b is a theoretical $(110)_\alpha$-pole figure calculated with both assumptions, i.e. Nishiyama-Wassermann (in the middle) and Kurdjumov-Sachs (on both sides) [11]. It matches quite well the experimental pole figure Figure 10a under the assumption that all intermediate orientations between the two models are also present. They fill an angular range of ~10.5° (continuously). The parallelism of the two close-packed planes $\{110\}_\alpha$ // $\{111\}_\gamma$ postulated in the two models is fulfilled very strictly, i.e. within ±1.5°. This result is based, on the one hand, on the availability of a sample in which phase transformation took place very near to the thermodynamic equilibrium (e.g. a meteorite) and, on the other hand, on an experimental technique with an angular resolving power much better than 1° (i.e. HE-synchrotron radiation).

Finally, we mention without, however, going into details that by combining several images of the type Figure 4b with different (hkl) the complete orientations $g_i = \{\varphi_1 \Phi \varphi_2\}_i$ of a large number of

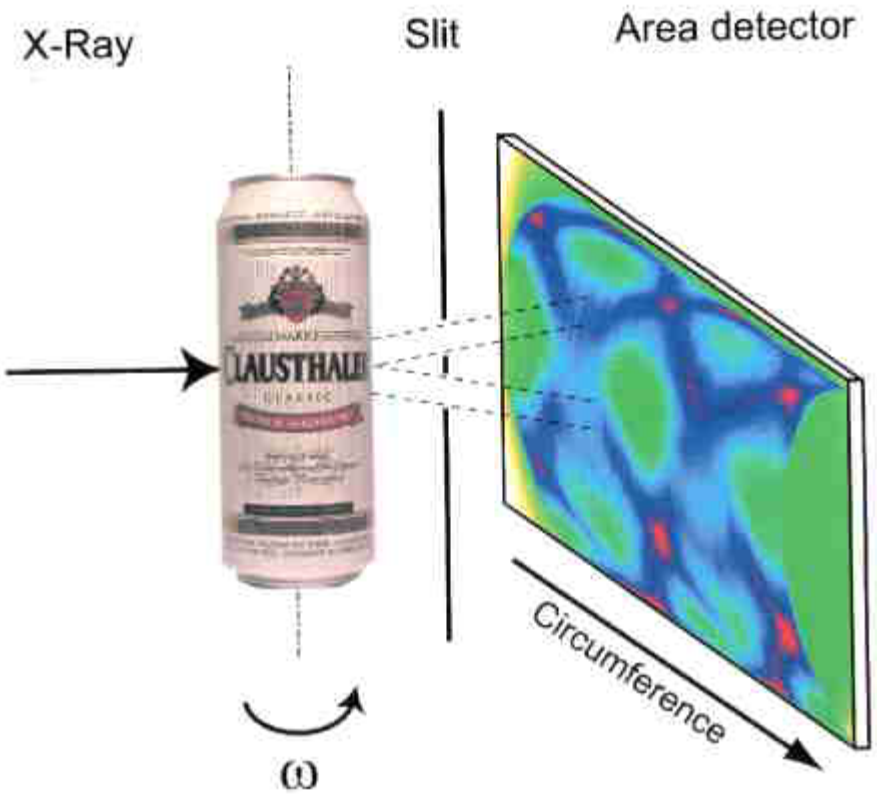

Figure 9. Texture inspection in a beverage can. The diffraction angle slit allows diffraction from one set of lattice planes (hkl) of the front- as well as the rear wall of the can to pass through. The can is rotated around its axis which images the texture variation along the circumference of the can (schematic).

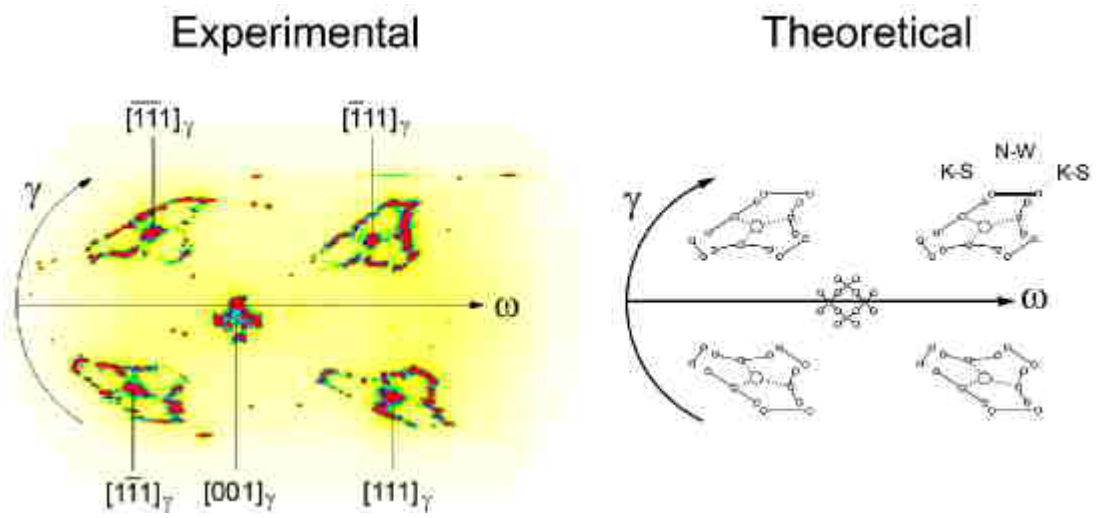

Figure 10. The (110)-pole figures of α-FeNi (Kamacite) of an octahedric meteorite of the Gibeon fall.
a) experimental; b) calculated with the models of Kurdjumov-Sachs and Nishiyama-Wassermann respectively, including all intermediate orientations between the two models.

crystallites of a polycrystalline sample can be obtained simultaneously. ("Tomography" in the orientation space) [12].

Also, by combining a sufficient number of images of type Figure 6 with different directions of the incident beam the complete position $\{x_1x_2x_3\}$ of a large number of grains can be obtained. Hence, in the case of *grain-resolved structures*, the complete six-dimensional *orientation stereology* [2] of the grains of the material can be revealed. The method is thus complementary to EBSD-scanning methods which can reveal orientation stereology only in the surface of the sample, but with much higher lateral resolution.

REFERENCES

[1] Bunge, H.J. (1982). *Texture Analysis in Materials Science*. Butterworths Publ. London.
[2] Bunge, H.J. & Schwarzer, R.A. (2001). Orientation Stereology – A New Branch in Texture Research. *Adv. Engin. Mater*. **3**, 25-39.
[3] Klein, H. & Bunge, H.J. (1999). Location Resolved Texture Analysis. Z. Metallkde. **90**, 103-110.
[4] Wcislak, L., Klein, H., Bunge, H.J., Garbe, U., Tschentscher, T. & Schneider, J.R. (2002). Texture Analysis with High-Energy Synchrotron Radiation. *J. Appl. Cryst*. **35**, 82-95.
[5] Bunge, H.J., Wcislak, L., Klein, H., Garbe, U. & Schneider, J.R. (2002). Texture and Microstructure Analysis with High-Energy Synchrotron Radiation. *Adv. Engin. Mater*. **4**, 300-304.
[6] Wassermann, G. & Grewen, J. (1962). *Texturen metallischer Werkstoffe*. Springer-Verlg, Berlin.
[7] Bouchard, R., Hupfeld, D., Lippmann, T., Neuefeind, J., Neumann, H.B., Poulsen, H.F., Rütt,U., Schmidt, T., Schneider, J.R., Sussenbach, J. & von Zimmermann, M. (1998). Triple-Crystal Diffractometer for High-Energy Synchrotron Radiation at the HASYLAB High-Field Wiggler Beamline BW5. *J. Synchr. Rad.* **5**, 90-101.

[8] Bunge, H.J., Wcislak, L., Klein, H., Garbe, U. & Schneider, J.R. (2003). Texture and Microstructure Imaging in Six Dimensions With High-Energy Synchrotron Radiation. *J. Appl. Cryst*. (submitted).
[9] Bunge, H.J. (2003). Über Meteoriten, Bierdosen und Synchrotronstrahlen. *TUContact (Clausthal)* **12**, 27-31.
[10] Weiss, W. & Bunge, H.J. (2001). Diffraction Contrast in X-ray Radiographic Images of Octahedric Meteorites. *J. Appl. Cryst*. **34**, 566-572.
[11] Bunge, H.J., Weiss, W., Klein, H., Wcislak, L., Garbe, U. & Schneider, J.R. (2003). Orientation Relationship of Widmannstätten Plates in an Iron Meteorite Measured With High-Energy Synchrotron Radiation. *J. Appl. Cryst*. **36**, 137-140.
[12] Bunge, H.J., Morris, P.R. & Nauer-Gerhardt, C.N. (1989). ODF-Analysis of Multipeak Textures. *Textures and Microstructures* **11**, 1-22.